The 1.5 Å Resolution Crystal Structure of $[Fe_3S_4]$-Ferredoxin from the Hyperthermophilic Archaeon *Pyrococcus furiosus*[†,‡]

Michael S. Nielsen, Pernille Harris,* Bee Lean Ooi, and Hans E. M. Christensen

Department of Chemistry, Building 207, Technical University of Denmark, DK-2800 Kgs. Lyngby, Denmark

Received January 8, 2004; Revised Manuscript Received March 4, 2004

ABSTRACT: The structure of $[Fe_3S_4]$-ferredoxin from the hyperthermophilic archaeon *Pyrococcus furiosus* has been determined to 1.5 Å resolution from a crystal belonging to space group $P2_1$ with two molecules in the asymmetric unit. The structure has been solved with molecular replacement by use of the ferredoxin from *Thermotoga maritima*. The fold is similar to that of related monocluster ferredoxins and contains two double-stranded antiparallel β-sheets and two α-helices. The hydrophobic interaction between Trp2 and Tyr46 is confirmed, linking the C-terminus to the longer α-helix. The structure contains a double-conformation disulfide bond existing in a left-handed and a right-handed spiral conformation. The crystal packing reveals a β-sheet interaction, which supports the suggestion that *P. furiosus* ferredoxin is a functional dimer. The extraordinary thermostability of *P. furiosus* ferredoxin is further discussed.

Iron−sulfur clusters are believed to have been a component of the first living organisms (*1*), which lived and developed under rather extreme conditions (*2*). The hyperthermophilic archaeon *Pyrococcus furiosus* (*P.f.*)[1] is an organism living under extreme conditions. It has a growth optimum at 100 °C and was originally isolated from submarine volcanic areas (*3*). It is a strictly anaerobic heterotroph, which harvests energy for growth from fermentation of carbohydrates through a modified Embden−Meyerhoff pathway (*4*). For electron transfer in this metabolic pathway, *P. furiosus* uses a small ferredoxin (7.5 kDa) comprising 66 amino acids and an iron−sulfur cluster (*5*).

The *P.f.* ferredoxin is one of the most studied ferredoxins, and it posseses several unique properties. The *P.f.* ferredoxin contains a single $[Fe_4S_4]$ cluster, which is coordinated by three cysteines and one aspartate (*5*). Aspartate ligation to an iron of the cluster is quite unusual. Among characterized single $[Fe_4S_4]$ cluster ferredoxins, this coordination is only seen so far in the ferredoxins from *P. furiosus* and *Thermococcus profundus* (*T.p.*) (*6*). The $[Fe_4S_4]$ cluster can be readily converted to the $[Fe_3S_4]$ cluster under oxidizing conditions, the labile iron-ion being the one originally coordinated to the aspartate (*5*).

The stability of *P.f.* ferredoxin, as well as the lability of the fourth iron, has made this protein especially attractive in studies involving formation of heterometallic clusters $[MFe_3S_4]$ where M = Ni^{2+}, Tl^{+}, Zn^{2+}, Co^{2+}, Mn^{2+}, Cd^{2+}, Cu^{+} and Cr^{2+} (*7*−*11*). In addition to this, a gallium-substituted *P.f.* ferredoxin containing a $[Ga_3S_4]$ cluster has been produced (*12*).

The *P.f.* ferredoxin is one of the most thermostable ferredoxins characterized, remaining unaffected after 12 h of incubation at 95 °C (*3*). The transition temperature of *P.f.* ferredoxin has unfortunately not been determined but it is believed to be higher than 125 °C, which is the transition temperature for the ferredoxin from *Thermotoga maritima* (*T.m.*), which has a growth optimum at 80 °C (*13*, *14*). However, a transition temperature between 176 and 195 °C has been estimated for *P.f.* rubredoxin from stability studies by H-exchange experiments (*15*).

P.f. ferredoxin has been investigated extensively by NMR, giving information on the electronic structure of the cluster (*16*−*19*) and the three-dimensional structure of the protein (*20*−*24*). The first investigations on the solution structure were done on the oxidized $[Fe_3S_4]$-ferredoxin and later on the $[Fe_4S_4]$-ferredoxin, leading to a preliminary molecular model (*24*). These investigations detected a folding pattern similar to those of *Desulfovibrio gigas* (*D.g.*) ferredoxin (*25*), *T.m.* ferredoxin (*13*), and *Thermococcus litoralis* (*T.l.*) ferredoxin (*26*), which was expected since the sequence identities with these are 43%, 49%, and 59%, respectively. By NMR, the disulfide bond between Cys21 and Cys48 has been shown to exist in two conformations, a left-handed and right-handed spiral conformation (*24*).

In the pursuit of the three-dimensional structure, *P.f.* ferredoxin has been crystallized as a complex with formaldehyde ferredoxin oxidoreductase, but the electron-density map showed a disordered ferredoxin structure except at the interface regions between the two proteins (*27*).

We report herein the three-dimensional structure of *P.f.* ferredoxin, containing the oxidized $[Fe_3S_4]$ cluster, determined by X-ray crystallography to 1.5 Å resolution.

MATERIALS AND METHODS

The gene encoding *P.f.* ferredoxin was expressed in *Escherichia coli* and the protein was purified according to

[†] H.E.M.C. was supported by the Danish Technical Science Research Council.

[‡] The coordinates have been deposited with the Brookhaven Protein Data Bank as entry 1SJ1.

* To whom corresponding should be addressed: Phone +45 45 25 20 24; fax +45 45 88 31 36; e-mail ph@kemi.dtu.dk.

[1] Abbreviations: *D.g.*, *Desulfovibrio gigas*; DPI, diffraction-component precision index; HEPES, *N*-(2-hydroxyethyl)piperazine-*N*′-(2-ethanesulfonic acid); PEG, poly(ethylene glycol); *P.f.*, *Pyrococcus furiosus*; *T.l.*, *Thermococcus litoralis*; *T.m.*, *Thermotoga maritima*; *T.p.*, *Thermococcus profundus*.

10.1021/bi049942x CCC: $27.50
Published on Web 04/17/2004

procedures published elsewhere (*28*). The [Fe_3S_4]-ferredoxin was crystallized by hanging-drop vapor diffusion as described (*29*). Data were collected on three crystals, one belonging to space group $P2_12_12_1$ and the others to $P2_1$ (*29*).

The orthorhombic crystal ($P2_12_12_1$) was crystallized with neomycin in solution with the hope of seeing neomycin in the structure (*28*, *29*). Furthermore, a data set was also collected to 1.75 Å on a crystal grown in the presence of neomycin (*29*), but the crystal was not of satisfactory quality and the data set has not been pursued further. Neomycin is not seen in any of the structures.

The monoclinic crystal ($P2_1$) was grown without neomycin in a reservoir solution containing 30% (w/v) PEG 400 and 0.1 M Tris-HCl, pH 8.0. The protein solution contained 6.5 mg of protein/mL and 20 mM Tris-HCl, pH 8.0. The drop was set up as a 2 + 2 μL drop, and 0.30 μL of 0.1 M $[Co(NH_3)_6]Cl_3$ was added to the drop. X-ray diffraction data to 1.5 Å resolution were collected at beamline ID14-4 at the European Synchrotron Radiation Facility (ESRF), Grenoble, France, and processed with the CCP4 program suite (*30*−*33*). The data suffered from a large anisotropic mosaicity.

The model of *P.f.* ferredoxin obtained from the orthorhombic crystal (PDB entry 1SIZ) (*29*) was used as a search model for the molecular replacement. This was carried out with MOLREP (*34*). A solution was found with two molecules in the asymmetric unit with a correlation coefficient of 0.51 and an *R*-factor of 0.44. The refinement of this solution was carried out with REFMAC5 (*35*) by use of CCP4i (*36*). The visual inspections and model rebuilding were carried out with the program *O* (*37*). Despite the high mosaic spread affecting the quality of the data (*29*), the electron density map is well-defined. The density for all the atoms in the cluster is seen as separate spheres with no trace of distortion. The only indication of the less satisfactory data is seen in the region around the [Fe_3S_4] cluster, as parallel slides of negative density separated with a constant distance. This is likely to be caused by data missing in part of the reciprocal space (the *c*-axis was almost coinciding with the rotation axis of the crystal). Four $[Co(NH_3)_6]^{3+}$ ions could be modeled into the electron densities, with two of the complex ions existing in a double conformation. The following residues were modeled with a double conformation: Val4, Thr10, Ser19, Cys21, Ile40, Cys48, and Glu65. The side chain of Glu65 seems to be quite flexible, where conformations a and b are the two outer conformations. The side chain of Asp9 in chain B could not be modeled. The disulfide bond between Cys21 and Cys48 was modeled in a left-hand spiral conformation with 40% occupancy and in a right-hand spiral conformation with 60% occupancy. The final model has an *R*-factor of 0.191 and an R_{free} of 0.219, and the model consists of two peptide chains Ala1−Ala66, two [Fe_3S_4] clusters, four $[Co(NH_3)_6]^{3+}$, and 152 water molecules. The refinement statistics are shown in Table 1. A Ramachandran plot was produced with PROCHECK (*38*) and showed that 92.4% of the ferredoxin residues were in the most favored region and 7.6% in the additional allowed regions.

RESULTS

Overall Structure of Pyrococcus furiosus Ferredoxin. The structure of *P.f.* ferredoxin containing the oxidized [Fe_3S_4] cluster and an intact disulfide bond was determined.

Table 1: Data Collection and Refinement Statistics[a]

Data Collection	
crystal space group	$P2_1$
resolution (Å)	34.6−1.50 (1.58−1.50)
unit cell parameters	
a (Å)	31.23
b (Å)	47.51
c (Å)	52.03
β (deg)	103.86
R_{merge}[b]	0.099 (0.305)
completeness (%)	89.8 (88.4)
$\langle I/\sigma(I)\rangle$	4.9 (2.2)
no. of reflections	76 346
no. of unique relcns.	21 276
redundancy	3.6 (3.7)
mosaicity[c] (deg)	1.0−1.7
Refinement	
resolution range	20−1.50
no. of reflections (working set/test set)	20 174/1087
R_{work}/R_{free} (%)	19.1/21.9
rms deviations from ideal geometry	
bond lengths (Å)	0.024
bond angles (deg)	2.03
No. of Atoms in Model	
protein	1118
ligands and ions	42
water oxygens	152

[a] Values in parentheses are for the highest resolution shell. [b] $R_{merge} = \Sigma_i \mid I_i - \langle I_i\rangle \mid / \Sigma_i I_i$, where $\langle I_i\rangle$ is the average of I_i over all symmetry equivalents. [c] From MOSFLM.

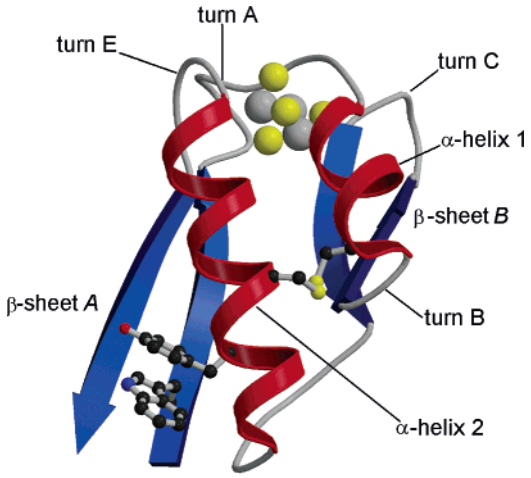

FIGURE 1: Overall fold of *P. furiosus* [Fe_3S_4]-ferredoxin. Turns A, B, C and E are marked, as well as α-helices 1 and 2 and β-sheets *A* and *B*. The π-stacking of Trp2 and Tyr46 is shown as well as the disulfide bond in the right-handed spiral conformation between residues Cys21 and Cys48. The figure was produced with Molscript and Raster3D (*45*, *46*).

The structure (Figure 1) confirms the general overall structure of monocluster ferredoxins (*14*, *25*). The shorter α-helix 1 involves residues Ala15−Pro22, while the longer α-helix 2 involves Cys42−Cys56. The structure contains two antiparallel β-sheets. β-sheet *B* is short, consisting of Val24−Asn28 and Lys32−Lys36. The longer β-sheet *A* is double-stranded, consisting of Ala1−Asp7 and Ala60−Ala66. The end of β-sheet *A* is tightly bound to α-helix 2 by the hydrophobic interaction between Trp2 and Tyr46 and by backbone hydrogen bonds between Trp2 and Ile40. The structure contains four reverse turns, A, B, C, and E. Turn D exists in the *T.m.* and *D.g.* ferredoxins but is not present in *P.f.* ferredoxin because of the insertion of four amino acids

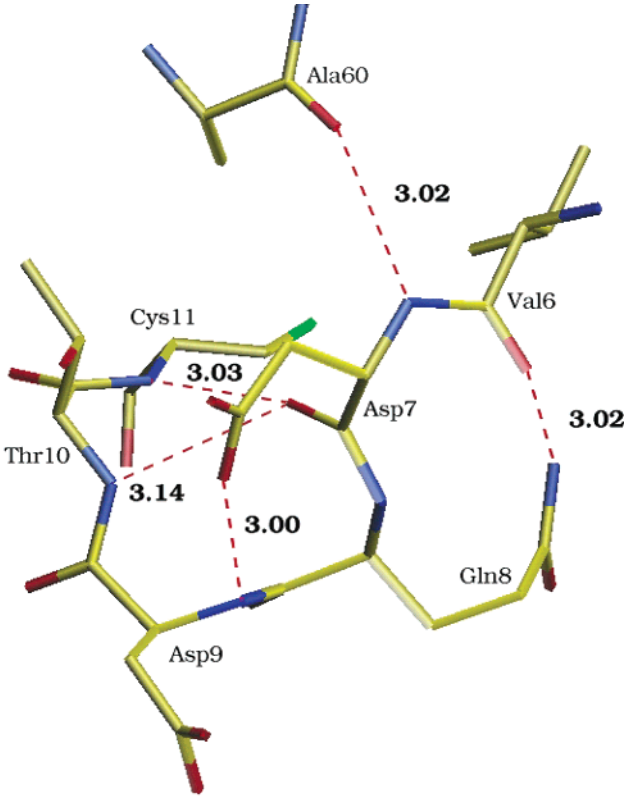

FIGURE 2: Highly hydrogen-cross-bonded turn A. Turn A is an Asx-type turn with Asp7 Oδ hydrogen-bonding to the NH of both residues Asp9 and Thr10. The turn also includes a hydrogen bond between Cys11 NH and O of Asp7, and the hydrogen bonding between Gln8 Nϵ and the carbonyl of Val6 further stabilizes the turn. The figure was produced in *O* (*37*).

producing a loop instead of a turn. Turn A is an Asx type I turn (*25*) involving Asp7−Cys11 (see Figure 2), where the carbonyl group of Asp7 has hydrogen bonds to the amino groups of both Thr10 and Cys11. Turn A is further stabilized by the hydrogen bonding of Val6 carbonyl group to the side-chain Nϵ2 of Gln8. Turn B is conserved in the *D.g.* and *T.m.* ferredoxins and is a variant of a type I turn since O of Cys21 is hydrogen-bonded to the amide groups of both Val24 and Phe25. Turn C is a type I Asx turn and turn E is an open type I turn. When the ferredoxin contains the $[Fe_4S_4]$ cluster, the fourth iron is coordinated by Asp 14 (*21*, *27*). In this structure the fourth iron is not present, and the side chain of Asp14 is turned away from the cluster and hydrogen-bonded to a water molecule. The distance from Asp14 N to S2 in the cluster is 3.6 Å, so the aspartate is located close to the missing iron and can easily turn to coordinate the fourth iron (see Figure 3).

The structure of *P.f.* ferredoxin is aligned (see Figure 4) with the structures of *T.m.* ferredoxin (PDB entry 1VJW) and *D.g.* ferredoxin (PDB entry 1FXD) by use of the program *O* (*37*). The largest deviations are seen in the N-terminal end of α-helix 2, where *P.f.* ferredoxin has four residues inserted compared to other similar ferredoxins (see Figure 4). Residues until *P.f.*-Glu41 and *T.m.*-Asp40 may be aligned. Then Asp42, Glu43, and Glu44 are inserted in the *P.f.* ferredoxin. *P.f.*-Leu45 and *T.m.*-Leu41 are very well aligned. Then comes an inserted Tyr46 followed by Asn47, which aligns with *T.m.*-Pro42. From the structural alignment it is evident that *P.f.*-Leu45 and *T.m.*-Leu40 are in the same

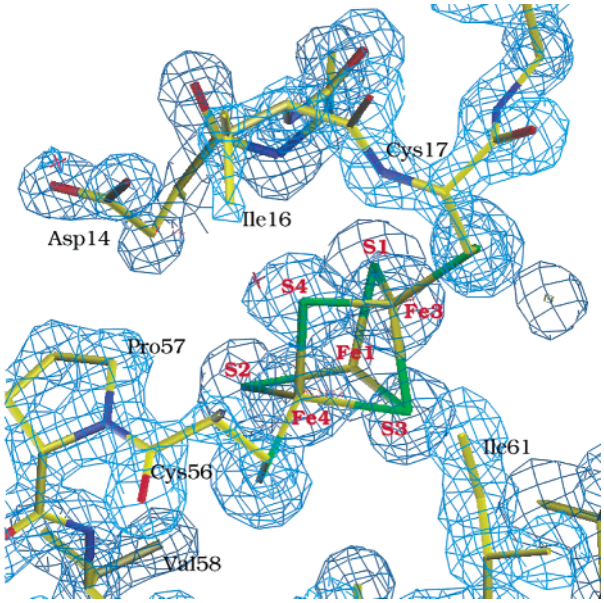

FIGURE 3: $2F_{obs} - F_{calc}$ σ-weighted electron density map (contoured at $\sigma = 1.9$) with the modeled $[Fe_3S_4]$ cluster and surrounding residues. Iron, yellow; sulfur, green. The figure was produced in *O* (*37*).

position. The position of Leu45 is conserved in several related ferredoxins and the Leu might have an important role in the disulfide bond environment and in the making of a hydrophobic core with residues Val24, Val37, and Ile40. The inserted residue Tyr46 is interacting with Trp2. This hydrophobic interaction is unprecedented in the related ferredoxins.

An estimation of the DPI of our structure according to Cruickshank (*39*) is 0.1 Å. We have listed H-bonding distances in Table 2. We generally find somewhat shorter hydrogen-bond distances than previously determined by NMR (*24*). Some distances differ quite significantly (see Table 2B); for example, there are no interactions between Val4 and Glu38. Thus we argue that β-sheet *A* should be described as a double-stranded β-sheet and not a triple-stranded β-sheet as proposed (*24*), since the two hydrogen bonds between Trp2 and Ile60 are the only hydrogen bonds that would make it triple-stranded. In turn E, the Ser59 N−Cys56 O distance is 0.5 Å longer than the distance determined by NMR. This might be due to the close proximity of a $[Co(NH_3)_6]^{3+}$ in the crystal packing (see Figure 5), which stabilizes a more open turn. In the NMR model for *P.f.* ferredoxin (*24*), turn E is described as significantly perturbed with the linkage between Ser59 and Ala60 being a cis peptide bond. The crystal structure, however, does not show a cis peptide bond but instead a trans peptide bond.

Cluster Environment. The cluster is coordinated by Fe−Sγ bonds to cysteines 11, 17, and 56. Except for the entrance to the empty site close to Asp14 where the fourth iron normally resides, the cluster is shielded from direct solvent contact by the backbone of residues 11−17 and by the hydrophobic side chains of Val6, Ile12, Ile16, Ala15, Phe25, Val58, and Ala60. Sulfurs 1, 2, and 4 in the cluster and Sγ of the cysteines participate in a NH···S hydrogen-bonding network that stabilizes the cluster (see Supporting Information), as also observed in the *D.g.* and *T.m.* ferredoxins (*14*, *25*). A water molecule is modeled close to S4 at approximately the position of the fourth iron. Water might

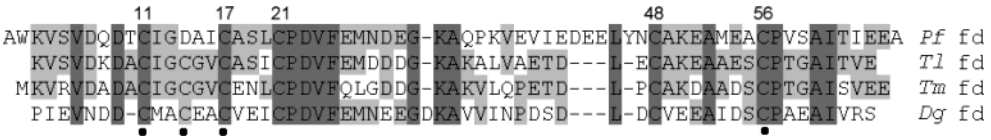

FIGURE 4: Structural sequence alignment of ferredoxins from *P. furiosus*, *T. maritima*, and *D. gigas*. The alignment of *T. litoralis* is based only upon the sequence. Leu45 is structurally aligned with Leu41 in *T.m.* ferredoxin. Strictly conserved residues are marked by dark gray, and those partly conserved are marked by light gray. ● marks the residues coordinating the cluster.

Table 2: Main-Chain Hydrogen Bonds in *P. furiosis* Ferredoxin and Comparison with Those Determined by NMR (*24*)

position	residues N	residues O	N···O (Å), this study chain A	N···O (Å), this study chain B	N···O (Å), NMR study (*24*)
(A) Possible Main-Chain Hydrogen Bonds					
β-sheet *A*	Ala1	Ala66	3.2	3.3	3.4
	Trp2	Ile40a	2.9	2.9	2.9
		Ile40b	3.1	3.0	
	Lys3	Glu64	2.9	2.9	2.9
	Ser5	Thr62	2.9	2.9	3.0
	Ile40	Trp2	2.9	2.8	3.4
	Thr62	Ser5	3.0	3.0	3.1
	Glu64	Lys3	2.8	2.9	3.4
	Ala66	Ala1	3.2	3.1	2.9
	Asp7	Ala60	3.0	3.0	
β-sheet *B*	Glu26	Gln34	3.0	3.1	3.4
	Asn28	Lys32	2.8	2.9	3.1
	Gln34	Glu26	2.9	2.9	3.2
	Lys36	Val24	2.7	2.7	3.4
	Gly31	Asn28	3.0	3.0	
helix 1	Cys17	Ala15	3.2	3.2	
	Ala18	Ala15	3.2	3.2	4.0
	Ser19	Ala15	3.1	3.1	3.4
	Leu20	Ile16	2.9	2.9	3.0
	Cys21a	Cys17	2.9	2.9	3.0
	Cys21b		2.9	2.9	
	Pro22	Ala18	3.1	3.2	
helix 2	Tyr46	Asp42	2.9	2.8	3.1
	Asn47	Glu43	2.9	2.8	2.8
	Cys48	Gln44	3.0	2.9	3.1
	Ala49	Leu45	3.0	2.9	3.0
	Lys50	Tyr46	2.9	2.9	2.7
	Glu51	Asn47	3.1	3.1	3.4
	Ala52	Cys48a	3.2	3.1	3.2
		Cys48b	2.9	2.9	
	Met53	Ala49	2.9	2.9	3.7
	Glu54	Lys50	3.0	3.0	3.8
	Ala55	Glu51	3.1	3.0	3.3
	Cys56	Ala52	3.1	3.1	
turn A	Asp7	Ala60	3.0	3.0	3.1
	Gln8	Val6	3.2	3.1	
	Asp9	Asp7	3.3	3.3	3.1
	Thr10a	Asp7	3.1	3.1	
	Thr10b		3.2	3.3	
	Cys11	Asp7	3.0	3.0	
turn B	Val24	Cys48a	3.0	3.1	3.2
		Cys48b	3.1	3.2	
	Phe25	Cys21	3.0	3.0	3.0
turn C	Gly31	Asn28	3.0	3.0	2.9
(B) Non-Hydrogen Bonds but Seen in the NMR Study as Possible Hydrogen Bonds					
β-sheet *A*	Val4	Glu38	5.5	5.4	2.8
turn A	Cys11	Gln8	4.0	4.0	3.5
	Thr10a	Gln8	3.5	3.6	3.5
	Thr10b		3.5	3.6	
turn E	Ser59	Cys56	3.5	3.5	3.0
loop	Val37	Ala24	4.3	4.4	3.6

be present in this position but the observed electron density could also be a result of the fourth iron being present in a small fraction of the ferredoxin molecules.

Disulfide Bond. Cys21 and Cys48 form a disulfide bond existing in an equilibrium between two conformations (*24*).

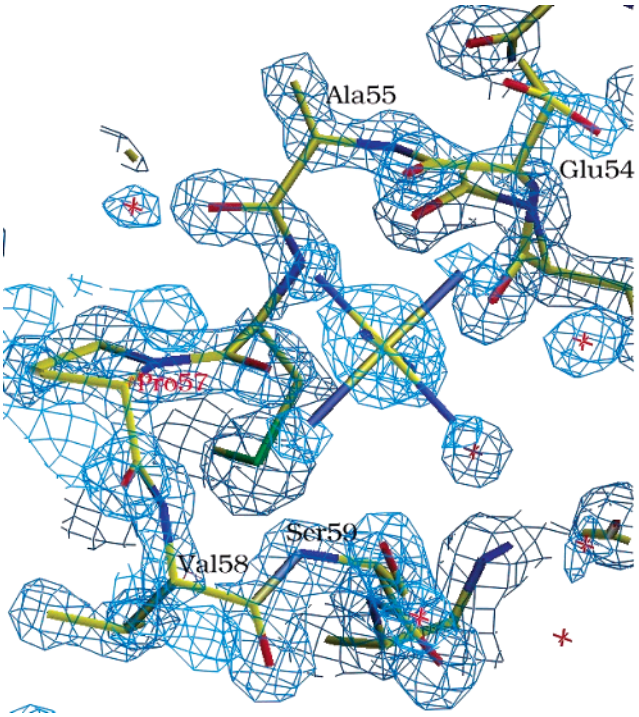

FIGURE 5: $2F_{obs} - F_{calc}$ σ-weighted electron density map (contoured at $\sigma = 1.6$) of turn E with the residues Cys56−Ser59 and the presence of $[Co(NH_3)_6]^{3+}$ close to the turn. The figure was produced in *O* (*37*).

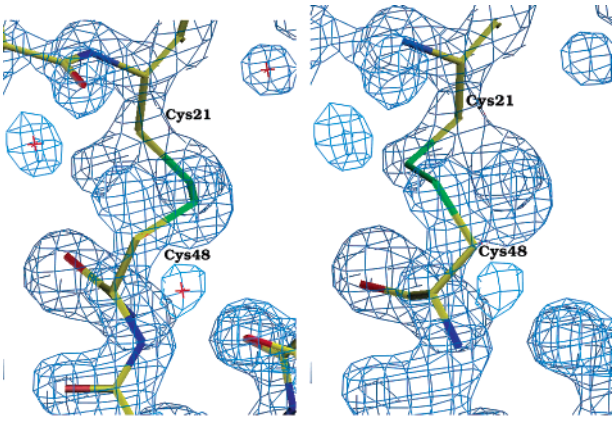

FIGURE 6: (a) Right-handed spiral disulfide bond of *P.f.* ferredoxin with a 60% occupancy. (b) Left-handed spiral disulfide bond with 40% occupancy. The figure was produced in *O* (*37*).

We find 60% of the disulfide bond in the right-handed spiral form and 40% in left-handed spiral form as shown in Figure 6. It has been proposed that the disulfide bond is destabilized by the extension of α-helix 2 at the amino terminal, compared to that of *T.m.* ferredoxin (*22*, *24*). The extension places Cys48 in the middle section of the helix, which causes unfavorable steric interactions between the Cys48 Sγ and the helix backbone (*22*, *24*). In the right-handed form the

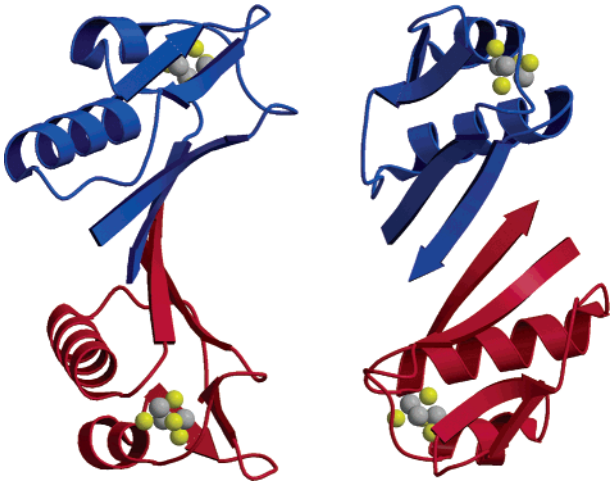

FIGURE 7: Overall structure of the suggested dimer of *P.f.* ferredoxin in different orientations. The figure was produced with Molscript (*45*).

distance between the Cys48 Sγ and of Leu45 O is 3.9 Å in both chains A and B, while the distance between the Cys48 Sγ the Leu45 Cα is 4.2 and 4.3 Å, respectively. These distances do not indicate a particularly strong repulsion of the Sγ away from the Leu45 as suggested earlier (*22*). It seems more likely that the destabilization of the right-handed disulfide bond is caused by the carbonyl group of Cys48, which is 3.6 Å from Cys21 Sγ in both chains A and B, or the vicinity of Val24, where the distance between Cys21 Sγ and Val Cγ2 is 3.4 and 3.2 Å, respectively. It can therefore not be concluded that the extension of α-helix 2 destabilizes the right-handed disulfide bond. The left-handed spiral disulfide bond is destabilized mainly by two interactions. When the disulfide bond is in the left-handed conformation, Cys48 Sγ is 2.7 and 2.9 Å away from Leu20 carbonyl O in chain A and B, respectively. Furthermore, Cys21 Sγ moves to a position that is 3.0 and 3.1 Å away from Cys48 O in chains A and B, respectively. It is clear, from these distances, that the left-handed spiral disulfide bond is destabilized relative to the right-handed.

The conversion between the two disulfide bond conformations in Cys21 is accommodated by a 105° rotation in χ_1. Therefore the hydrogen bonding between Cys21 N and the carbonyl of Cys17, which is in direct contact with the cluster, is not disturbed. In Cys48, the conversion between the two disulfide bond conformations is not only a mere rotation in χ_1 but also a movement in the backbone of Cys48 (see Figure 6). The movement in Cys48 does not perturb the α-helix 2 significantly, but it changes the length of the hydrogen bonds between Cys48 and Ala52 (see Table 2).

Dimerization. Some uncertainty exists as to whether *P.f.* ferredoxin functions as a dimer. It was recently proposed that this ferredoxin is a dimer at physiological ionic strength, i.e., at approximately 0.35 M NaCl (*40*). The crystal packing reveals two possible ways of dimerization. One is the interface, which has two $[Co(NH_3)_6]^{3+}$ linking the two monomers and will therefore be physiologically irrelevant. The other possibility is the β-sheet interactions between Ile63 and Glu65 (a table of hydrogen bonds can be seen in Supporting Information). These interactions form an extended β-sheet between the two β-sheets *A*, which results in a half β-barrel structure (see Figure 7). In addition to the main-chain interactions, side-chain hydrogen bonding exists involving Tyr46 OH, Glu65 Oϵ1+2, and Ile63 O. In chain B the position of Lys50 Nζ suggests a possible salt bridge between Lys50 and Glu65 Oϵ1. On the other hand, in chain A, Lys50 Nζ points away from Glu65, indicating the absence of a salt bridge. The distance between the two $[Fe_3S_4]$ clusters is 34.3 Å from Fe3 to Fe3′. Since oligomerization of proteins often increases their thermostability by reducing the surface/volume ratio (*41*−*43*) and there is a possibility that the *P.f.* ferredoxin is a dimer, the β-sheet dimerization could be of physiological relevance. Furthermore, the β-sheet interaction also shields Met53 from the solvent, making it more resistant to high-temperature oxidation.

Table 3: Comparison of the Number of H-Bonds in *Pyrococcus furiosus* and *Thermotoga maritima* Ferredoxins

ferredoxin	no. of residues	total no. of H-bonds	main-chain H-bonds	salt bridges	side-chain H-bonds	charge-neutral H-bonds
P.f.	66	58	39	1	19	10
T.m.	60	43	29	1	14	9

Factors Increasing Thermostability. The thermostability of *P.f.* ferredoxin is extraordinary, and *P.f.* ferredoxin is believed to be more thermostable than *T.m.* ferredoxin (T_{opt} = 80 °C) (*18*). It would therefore be of interest to examine the factors that give rise to the higher thermostability of *P.f.* ferredoxin as compared to *T.m.* ferredoxin. The overall structure of these two ferredoxins is essentially the same, although *P.f.* ferredoxin is 6 residues longer and contains structural extensions in α-helix 2 and in the β-sheet of the two termini. There is an increase in the number of hydrogen bonds in *P.f.* ferredoxin compared to *T.m.* ferredoxin, even when the larger number of residues is taken into account. In *T.m.* ferredoxin there are 43 H-bonds, while there are 58 in *P.f.* ferredoxin (see Table 3), which contributes to the increased thermostability. Salt bridges are generally believed to increase the thermostability (*43*). However, there is only one salt bridge in the *P.f.* and *T.m.* ferredoxins (*14*). In *T.m.* ferredoxin there is a salt bridge between Glu38 Oϵ2 and the amino terminus, while in *P.f.* ferredoxin a possible salt bridge is found between the terminal carboxyl group of Ala66 and the amino group of Ala1. The N···O distance is 3.2 and 3.3 Å for the two chains, which indicates a relatively weak salt bridge.

The hydrophobic interaction between Trp2 and Tyr46 is unprecedented in other ferredoxins and has an important stabilizing effect (Figure 1). This π-stacking with an aromatic ring separation of 3.5 Å holds the terminal ends of β-sheet *A* to α-helix 2 and could be important in sustaining the compactness of the protein at high temperatures.

Helix capping stabilizes the α-helix structure (*44*), and the N-terminal end of α-helix 2 is stabilized by hydrogen bonding between the side chain of Asp42 and NH groups of Glu44 and Leu45 (see Figure 8). This kind of side-chain helix capping is not seen in the related *T.m.* and *D.g.* ferredoxins and may also contribute to the thermostability of *P.f.* ferredoxin.

As in the case of *T.m.* ferredoxin (*14*), some of the turns in *P.f.* ferredoxin are highly stabilized by side-chain interactions (Asx type). Turn A (see Figure 2) is highly cross-linked to the side chains of Asp7 and Gln8. In turn C, Asn28 Oδ1 hydrogen-bonds to NH of both Glu30 and Lys32, in addition

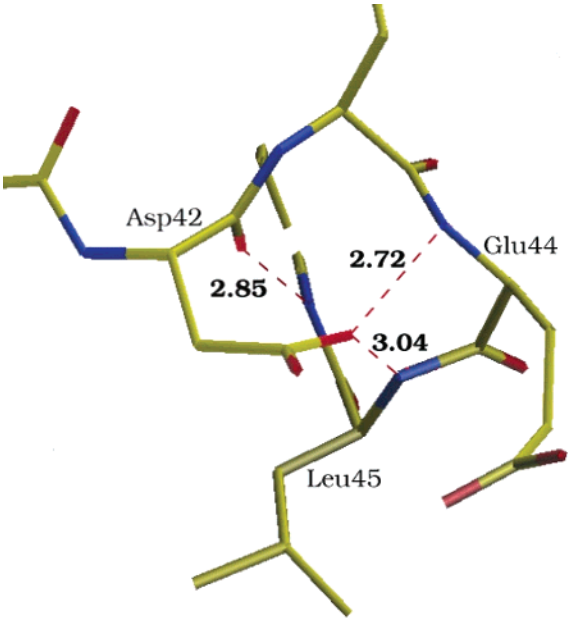

FIGURE 8: Helix capping of α-helix 2 by the Asp42 side chain, hydrogen-bonding to NH of Glu44 and NH of Leu45. The figure was produced in *O* (*37*).

to the backbone hydrogen bond between Gly31 NH and Asn28 O. Furthermore, the Asn28 Nδ2 is also hydrogen-bonded to both Oϵ1 of Gln8 and Gln34. This gives a highly stabilized hydrogen-bond network. Turns B and E are stabilized as in *T.m.* ferredoxin. Generally the stabilization of the turns is similar to that of *T.m.* ferredoxin and is therefore not a contributing factor in a possible difference in thermostability between the *T.m.* and *P.f.* ferredoxins.

In summary, a high-resolution structure of *P.f.* [Fe_3S_4]-ferredoxin has been determined. The structure shows a disulfide bond in two conformations, and possible interactions giving rise to formation of a dimer have been proposed. The structure shows a higher degree of hydrogen-bond network than other related ferredoxins, which is believed to be the main reason for the increased thermostability of this hyperthermostable ferredoxin.

ACKNOWLEDGMENT

Jens-Christian N. Poulsen, Heidi A. Ernst, Eva Johansson, and Flemming Hansen from University of Copenhagen are acknowledged for help with the crystallization and data collection. We acknowledge the European Synchrotron Radiation Facility for provision of synchrotron radiation facilities and thank Didier Nurizzo for assistance in using beamline ID14-4. Financial support to M.S.N. from the Novo Scholarship Program is acknowledged.

SUPPORTING INFORMATION AVAILABLE

Tables of hydrogen-bond distances; main-chain to side-chain, side-chain to side-chain, and NH···S bonding distances; and dimeric hydrogen-bonding distances. This material is available free of charge via the Internet at http://pubs.acs.org.

REFERENCES

1. Beinert, H. (2000) Iron−sulfur proteins: ancient structures, still full of surprises, *J. Biol. Inorg. Chem. 5*, 2−15.
2. Woese, C. R., Kandler, O., and Wheelis, M. L. (1990) Towards a natural system of organisms: proposal of the domains archaea, bacteria and eucarya, *Proc. Natl. Acad. Sci. U.S.A. 87*, 4576−4579.
3. Aono, S., Bryant, F. O., and Adams, M. W. W. (1989) A novel and remarkably thermostable ferredoxin from the hyperthermophilic archaebacterium *Pyrococcus furiosus*, *J. Bacteriol. 171*, 3433−3439.
4. Kengen, S. W. M., de Bok, F. A. M., van Loo, N., Dijkema, C., Stams, A. J. M., and de Vos, W. M. (1994) Evidence for the operation of a novel Embden-Meyerhof pathway that involves ADP-dependent kinases during sugar fermentation by *Pyrococcus furiosus*, *J. Biol. Chem. 269*, 17537−17541.
5. Conover, R. C., Kowal, A. T., Fu, W., Park, J.-B., Aono, S., Adams, M. W. W., and Johnson, M. K. (1990) Spectroscopic characterization of the novel iron−sulfur cluster in *Pyrococcus furiosus* ferredoxin, *J. Biol. Chem. 265*, 8533−8541.
6. Imai, T., Taguchi, K., Ogawara, Y., Ohmori, D., Yamakura, F., Ikezawa, H., and Urushiyama, A. (2001) Characterization and cloning of an extremely thermostable, *Pyrococcus furiosus*-type 4Fe ferredoxin from *Thermococcus profundus*, *J. Biochem. (Tokyo) 130*, 649−655.
7. Conover, R. C., Park, J. B., Adams, M. W. W., and Johnson, M. K. (1990) Formation and properties of a $NiFe_3S_4$ cluster in *Pyrococcus furiosus* ferredoxin, *J. Am. Chem. Soc. 112*, 4562−4564.
8. Fu, W., Telser, J., Hoffman, B. M., Smith, E. T., Adams, M. W. W., Finnegan, M. G., Conover, R. C., and Johnson, M. K. (1994) Interaction of Tl^+ and Cs^+ with the [Fe_3S_4] cluster of *Pyrococcus furiosus* ferredoxin: investigation by Resonance Raman, MCD, EPR, and ENDOR spectroscopy, *J. Am. Chem. Soc. 116*, 5722−5729.
9. Finnegan, M. G., Conover, R. C., Park, J. B, Zhou, Z. H., Adams, M. W. W., and Johnson, M. K. (1995) Electronic, magnetic, redox, and ligand-binding properties of [MFe_3S_4] clusters (M = Zn, Co, Mn) in *Pyrococcus furiosus* ferredoxin, *Inorg. Chem. 34*, 5358−5369.
10. Staples, C. R., Dawan, I. K., Finnegan, M. G., Dwinell, D. A., Zhou, Z. H., Huang, H., Verhagen, M. F. J. M., Adams, M. W. W., and Johnson, M. K. (1997) Electronic, magnetic, redox properties of [MFe_3S_4] clusters (M = Cd, Cu, Cr) in *Pyrococcus furiosus* ferredoxin, *Inorg. Chem. 36*, 5740−5749.
11. Fawcett, S. E. J., Davis, D., Breton, J. L., Thomson, A. J., and Armstrong, F. A. (1998) Voltammetric studies of the reactions of iron-sulphur clusters ([3Fe-4S] or [M3Fe-4S]) formed in *Pyrococcus furiosus* ferredoxin, *Biochem. J. 335*, 357−368.
12. Johnson, K. A., Brereton, P. S., Verhagen, M. F. J. M., Calzolai, L., La Mar, G. N., Adams, M. W. W., and Amster, I. J. (2001) A gallium-substituted cubane-type cluster in *Pyrococcus furiosus* ferredoxin, *J. Am. Chem. Soc. 123*, 7935−7936.
13. Pfeil, W., Gesierich, U., Kleemann, G. R., and Sterner, R. (1997) Ferredoxin from the hyperthermophile *Thermotoga maritima* is stable beyond the boiling point of water, *J. Mol. Biol. 272*, 591−596.
14. Marcedo-Ribeiro, S., Darimont, B., Sterner, R., and Huber, R. (1996) Small structural changes account for the high thermostability of 1[4Fe-4S] ferredoxin from the hyperthermophile bacterium *Thermotoga maritima*, *Structure 4*, 1291−1301.
15. Hiller, R., Zhou, Z. H., Adams, M. W. W., and Englander, W. (1997) Stability and dynamics in a hyperthermophilic protein with melting temperature close to 200 °C, *Proc. Natl. Acad. Sci. U.S.A. 94*, 11329−11332.
16. Busse, S. C., La Mar, G. N., Yu, L. P., Howard, J. B., Smith, E. T., Zhou, Z. H., and Adams, M. W. W. (1992) Proton NMR investigation of the oxidized three-iron clusters in the ferredoxins from the hyperthermophilic archae *Pyrococcus furiosus* and *Thermococcus litoralis*, *Biochemistry 31*, 11952−11962.
17. Gorst, C. M., Zhou, Z. H., Ma, K., Teng, Q., Howard, J. B., Adams, M. W. W., and La Mar, G. N. (1995) Participation of the disulfide bridge in the redox cycle of the ferredoxin from the hyperthermophilic *Pyrococcus furiosus*: ^1H nuclear magnetic resonance time resolution of the four redox states at ambient temperature, *Biochemistry 34*, 8788−8795.
18. Calzolai, L, Zhou, Z. H., Adams, M. W. W., and La Mar, G. N. (1996) Role of cluster-ligated aspartate in gating electron transfer in the four-iron ferredoxin from the hyperthermophile archaeon *Pyrococcus furiosus*, *J. Am. Chem. Soc. 118*, 2513−2514.
19. Calzolai, L., Gorst, C. M., Bren, K. L., Zhou, Z. H., Adams, M. W. W., and La Mar, G. N. (1997) Solution NMR study of the

electronic structure and magnetic properties of cluster ligation mutants of the four-iron ferredoxin from the hyperthermophile archaeon *Pyrococcus furiosus*, *J. Am. Chem. Soc. 119*, 9341−9350.
20. Teng, Q., Zhou, Z. H., Smith, E. T., Busse, S. C., Howard, J. B., Adams, M. W. W., and La Mar, G. N. (1994) Solution ^{1}H NMR determination of secondary structure for the three-iron form of ferredoxin from the hyperthermophilic archaeon *Pyrococcus furiosus*, *Biochemistry 33*, 6316−6326.
21. Calzolai, L., Gorst, C. M., Zhao, Z.-H., Teng, Q., Adams, M. W. W., and La Mar, G. N. (1995) ^{1}H NMR investigation of the electronic and molecular structure of the four iron cluster ferredoxin from the hyperthermophile *Pyrococcus furiosus*. Identification of Asp 14 as a cluster ligand in each of the four redox states, *Biochemistry 34*, 11373−11384.
22. Wang, P., Calzolai, L., Bren, K. L., Teng, Q., Jenney, F. E., Jr., Brereton, P. S., Howard, J. B., Adams, M. W. W., and La Mar, G. N. (1999) Secondary structure extensions in *Pyrococcus furiosus* ferredoxin destabilize the disulfide bond relative to that in other hyperthermostable ferredoxins. Global consequences for the disulfide orientational heterogeneity, *Biochemistry 38*, 8167−8178.
23. Webba da Silva, M., Sham, S., Gorst, C. M., Calzolai, L., Brereton, P. S., Howard, J. B., Adams, M. W. W., and La Mar, G. N. (2001) Solution NMR characterization of the thermodynamics of the disulfide bond orientational isomerism and its effect of cluster electronic properties for the hyperthermostable three-iron cluster ferredoxin from the archaeon *Pyrococcus furiosus*, *Biochemistry 40*, 12575−12583.
24. Sham, S., Calzolai, L., Wang, P., Bren, K., Haarklau, H., Brereton, P. S., Adams, M. W. W., and La Mar, G. N. (2002) A solution NMR molecular model for the aspartate-ligated, cubane cluster containing ferredoxin from the hyperthermophilic archaeon *Pyrococcus furiosus*, *Biochemistry 41*, 12498−12508.
25. Kissenger, C. R., Sieker, L. C., Adman, E. T., and Jensen, L. H. (1991) Refined crystal structure of ferredoxin II from *Desulfovibrio gigas* at 1.7 Å, *J. Mol. Biol. 219*, 693−715.
26. Wang, P., Donaire, A., Zhou, Z. H., Adams, M. W. W., and La Mar, G. N., (1996) Molecular model of the solution structure for the paramagnetic four-iron ferredoxin from the hyperthermophilic archaeon *Thermococcus litoralis*, *Biochemistry 35*, 11319−11328.
27. Hu, Y., Faham, S., Roy, R., Adams, M. W. W., and Rees, D. C. (1999) Fomaldehyde ferredoxin oxidoreductase from *Pyrococcus furiosus*: The 1.85 Å resolution crystal structure and its mechanistic implications, *J. Mol. Biol. 286*, 899−914.
28. Barat-Jankovics, H., Ooi, B. L., Christophersen, S., Nielsen, M. S., Siu, Y. S., and Christensen, H. E. M. To be published.
29. Nielsen, M. S., Harris, P., and Christensen, H. E. M. (2003) Crystallization of [Fe_3S_4]-ferredoxin from the hyperthermophile archaeon *Pyrococcus furiosus*, *Acta Crystallogr. D59*, 2325−2327.
30. Leslie, A. G. W. (1992) *Jnt. CCP4/ESF-EACMB Newslett. Protein Crystallogr. 26*.
31. Evans, P. R. (1993). *Proceedings of the CCP4 Study Weekend. Data Collection and Processing* (Sawyer, L., Isaacs, N., and Bailey, S., Eds.) pp 114−122, Daresbury Laboratory, Warrington, U.K.
32. Collaborative Computational Project, Number 4 (1994) The *CCP*4 suite: Programs for protein crystallography, *Acta Crystallogr. D50*, 760−763.
33. French, G. S., and Wilson, K. S. (1978) On the treatment of negative intensity observations, *Acta Crystallogr. A34*, 517−525.
34. Vagin, A., and Teplyakov, A. (1997) *MOLREP*: an automated program for molecular replacement, *J. Appl. Crystallogr. 30*, 1022−1025.
35. Murshudov, G. N., Vagin, A. A., and Dodson, E. J. (1997) Refinement of macromolecular structures by the maximum-likelihood method, *Acta Crystallogr. D53*, 240−255.
36. Potterton, E., Briggs, P., Turkenburg, M., and Dodson, E. (2003) A graphical user interface to the *CCP*4 program suite, *Acta Crystallogr. D59*, 1131−1137.
37. Jones, T. A., Zou, J.-Y., Cowan, S. W., and Kjeldgaard, M. (1991) Improved methods for building protein models in electron density maps and the location of errors in the models, *Acta Crystallogr. A47*, 110−119.
38. Laskowski, R. A., MacArthur, M. W., Moss, D. S., and Thornton, J. M. (1993) PROCHECK: a program to check the stereochemical quality of protein structures, *J. Appl. Crystallogr. 26*, 283−291.
39. Cruickshank, D. W. J. (1999) Remarks about protein structure precision, *Acta Crystallogr. D55*, 583−601.
40. Hasan, M. N., Hagedoorn, P. L., and Hagen, W. R. (2002) *Pyrococcus furiosus* ferredoxin is a functional dimer, *FEBS Lett. 531*, 335−338.
41. Russel, R. J. M., Ferguson, J. M. C., Hough, D. W., Danson, M. J., and Taylor, G. L. (1997) The crystal structure of citrate synthase from the hyperthermophilic archaeon *Pyrococcus furiosus* at 1.9 Å resolution, *Biochemistry 36*, 9983−9994.
42. Massant, J., Wouters, J., and Glansdorff, N. (2003) Refined structure of *Pyrococcus furiosus* ornithine carbamoyltransferase at 1.87 Å, *Acta Crystallogr. D59*, 2140−2149.
43. Kumar, S., Tsai, C.-J., and Nussinov, R. (2000) Factors enhancing protein thermostability, *Protein Eng. 13*, 179−191.
44. Aurora, R., and Rose, G. D. (1998) Helix capping, *Protein Sci. 7*, 21−38.
45. Kraulis, P. J. (1991) MOLSCRIPT: A program to produce both detailed and schematic plots of protein structures, *J. Appl. Crystallogr. 24*, 946−950.
46. Merritt, E. A., and Bacon, D. J. (1997), Raster3D Photorealistic Molecular Graphics, *Methods Enzymol. 277*, 505−524.

BI049942X